Proceedings of the 17th World Congress
The International Federation of Automatic Control
Seoul, Korea, July 6-11, 2008

An integrated chassis controller for automotive vehicle emulation ⋆

Mehmet Akar * **Jens C. Kalkkuhl** **

* *Department of Electrical and Electronic Engineering*
Boğaziçi University, Bebek, 34342, İstanbul Turkey
Tel: +90 212 3596466; E-mail: mehmet.akar@boun.edu.tr
** *Daimler AG, Sindelfingen, Germany*

Abstract: This paper discusses an integrated chassis controller for vehicle emulation. The proposed scheme consists of 4–wheel automatic steering for lateral dynamics tracking, and a suspension controller for emulating desired vertical motion. The lateral controller is designed based on the observation that the coupling from vertical to lateral dynamics is weak in the linear operating regime of interest (i.e., for lateral accelerations below $4m/s^2$), whereas the suspension controller compensates for the coupling from lateral to vertical dynamics. The efficacy of the proposed method is demonstrated by realistic experiments in an advanced nonlinear simulator.

1. INTRODUCTION

Vehicle emulation has been an important concept in the development of a generic prototype test vehicle [Lee, 1995]. Sophisticated control algorithms together with advanced actuators are needed to make an automotive vehicle drive like another. In this context, automatic 4-wheel steering is essential in tracking desired lateral dynamics, whereas a properly equipped and controlled suspension system is required to provide the flexibility in tracking the desired vertical motion generated by a reference vehicle. There is a vast amount of literature on active steering to control vehicle lateral dynamics [see Furukawa et al., 1989; Akar, 2006; and the references therein]. Similarly, quite a lot of work has been done on active suspension control for improving comfort and road safety [Yamashita et al., 1990; Duplitzer, 1996; Hrovat, 1997; Magnus, 2001; Smith and Wang, 2002]. This paper presents an an *integrated chassis controller* (ICC) for the specific problem of vehicle emulation. The proposed controller is for a compact size test vehicle that is equipped with 4–wheel (4W) steering and active hydro–pneumatic suspension (AHP).

The general schematic of the vehicle emulation concept that is of interest in this paper is given in Fig. 1. As shown, the driver commands the reference vehicle which produces desired trajectories for lateral motion that are characterized in terms of side slip angle and yaw rate; and desired lift/roll/pitch angles for vertical motion. Our task is to generate the steering angles and the input currents for the AHP system on each tire so that the state variables of the test vehicle follow those of the reference vehicle.

The proposed integrated controller structure is also shown in Fig. 1. Our approach to vehicle emulation is to use a decoupled design perspective, i.e., utilize 4W–steering for lateral tracking, and the suspension system for vertical motion control. A key consideration in adapting this decentralized strategy is to minimize the number of signals to be shared between the lateral and the vertical subsystems. Since we are interested in the linear operating regime of vehicles (i.e., for lateral accelerations below $4m/s^2$), this approach is further justified due to weak coupling from vertical dynamics to lateral ones. Next, we move onto more detailed descriptions of the 4W steering and the suspension units.

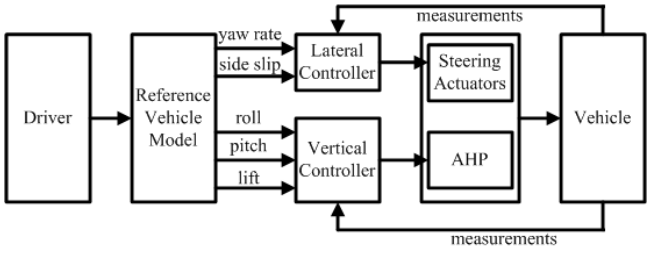

Fig. 1. Vehicle Emulation Schematic

2. LATERAL DYNAMICS CONTROL

The reference and test vehicles are both represented using the single track model, and the equations of motion can be compactly characterized by the state space model [1]

$$\dot{x} = Ax + Bu + Ew, \tag{1}$$

where x is the state vector, u contains the steering inputs, and w denotes the unmeasurable wind disturbance, and

$$x = \begin{bmatrix} \beta \\ \dot{\psi} \end{bmatrix}, \; u = \begin{bmatrix} \delta_v \\ \delta_h \end{bmatrix}, \tag{2}$$

$$A = \begin{bmatrix} -\dfrac{C_v + C_h}{mv_x} & \dfrac{C_v l_v - C_h l_h}{mv_x^2} + 1 \\ \dfrac{C_v l_v - C_h l_h}{J_z} & -\dfrac{C_v l_v^2 + C_h l_h^2}{J_z v_x} \end{bmatrix}, \tag{3}$$

⋆ This work was supported in part by EU FP6 Project CEmACS 004175 and BAP 07HA202.

[1] Nomenclature for parameters in Table I.

m	Vehicle mass
C_v, C_h	Front and rear linear tire stiffness parameters
l_v, l_h	Longitudinal position of center of gravity measured from front and rear axles
L	Axle separation ($L = l_v + l_h$)
J_z	Yaw moment of inertia
v_x, v_y	Longitudinal and lateral velocities measured at the vehicle center of gravity
l_w	Distance between the center of gravity and the point of impact of disturbance (wind)
β	Sideslip angle at the vehicle center of gravity
$\dot{\psi}$	Yaw rate
δ_v	Steering angle at the front wheel
δ_h	Steering angle at the rear wheel
w	Disturbance (wind)

Table 1. Nomenclature for lateral dynamics

$$B = \begin{bmatrix} -\dfrac{C_v}{mv_x} & -\dfrac{C_h}{mv_x} \\ \dfrac{C_v l_v}{J_z} & -\dfrac{C_h l_h}{J_z} \end{bmatrix}, \; E = \begin{bmatrix} \dfrac{1}{mv_x} \\ \dfrac{-l_w}{J_z} \end{bmatrix}. \qquad (4)$$

The above model we adopt in the design of the 4W–steering unit ignores the weak coupling from the vertical dynamics. A more accurate mathematical description would include the additional term, $h\ddot{\phi}/v_x$, in the state equation for the side slip angle, where h is the center of gravity height, and ϕ is the roll angle. However, in the linear operating regime of the compact size test vehicle of interest, it is not difficult to verify by simulation that the two models produce very close side slip angles and yaw–rates. Furthermore, given that there is uncertainty in vehicle parameters, and measured value of the roll acceleration, compensating for the vertical dynamics using the lateral controller does not seem to be a reasonable approach. Taking all of the above–mentioned criteria into account, we choose to use (1) in the design of the 4W–steering unit.

2.1 Lateral Controller Design

The task of the lateral controller is to help track the given reference trajectory $[\beta_{ref}(t), \dot{\psi}_{ref}(t)]^T$, as closely as possible despite the existence of unmeasurable wind disturbance. For the lateral controller description in the sequel, we assume that the vehicle states $(\beta(t), \dot{\psi}(t))$ are available. Note that $\dot{\psi}(t)$ can be measured using standard sensors, but $\beta(t)$ may be obtained using either a nonlinear observer or a Kalman filter. In the simulation results to be presented in Section 4, this state variable is obtained through a Kalman filter.

In this paper, the lateral dynamics tracking is achieved using a sliding mode theory based controller. To this end, let the sliding manifold be $\sigma_L = 0$, where

$$\sigma_L(t) = \dot{e}_L(t) + \lambda_{L1} e_L(t), \qquad (5)$$

$$e_L(t) = \begin{bmatrix} \beta(t) - \beta_{ref}(t) \\ \dot{\psi} - \dot{\psi}_{ref} \end{bmatrix}. \qquad (6)$$

If the state trajectories are already restricted to the sliding manifold $\sigma_L(t) = 0$, note that the sliding motion is given by $\dot{e}_L(t) = -\lambda_{L1} e_L(t)$; therefore, we are guaranteed to have stable sliding motion if the gain matrix λ_{L1} is chosen to have eigenvalues in the right half of the complex plane.

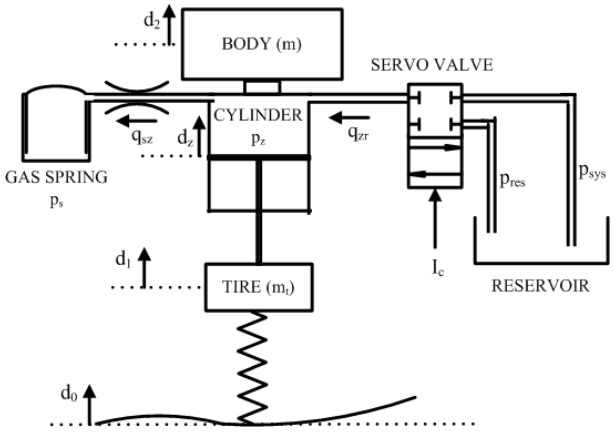

Fig. 2. AHP diagram for a quarter car

Thus, it remains to determine steering inputs u such that the manifold is reached in finite time.

Note that the vehicle parameters are known to a certain accuracy level in the general case. For instance, loading and road conditions all affect m, J_z, l_v, l_h, C_v, and C_h, whereas different tires on the vehicle may lead to additional variations in C_v and C_h. Therefore, instead of their exact values for A, B, and E, assume that we only have estimates A_n, B_n, and E_n which can be used in the controller design. Now consider the sliding mode controller

$$u = B_n^{-1} \left(\dot{x}_{ref} - A_n x - \lambda_{L1} e_L - \lambda_{L2} \sigma_L - M_n \mathrm{sgn}(\sigma_L) \right) (7)$$

where the gain matrices M_n and λ_{L2} are to be chosen such that the trajectories are directed towards the manifold $\sigma_L = 0$. Indeed this can be achieved by choosing λ_{L2} to have eigenvalues in the right half plane, and M_n sufficiently high.

3. VERTICAL DYNAMICS CONTROL

Automobile suspensions are designed for enhanced ride comfort and handling. Conventional passive suspensions achieve these conflicting purposes through the use of springs and dampers. In an active suspension system that is the topic of this paper, the required forces are generated through active elements such as hydraulic pumps [Yamashita et al., 1990; Duplitzer, 1996; Hrovat, 1997; Magnus, 2001; Smith and Wang, 2002; Akar et al., 2007]. In this section, we outline the details of our integrated active suspension controller for vertical dynamics emulation. The proposed controller consists of an active body controller and a force controller, that are both designed based on mathematical models derived from the physics of the system and also validated by experimental data. The active body controller design draws heavily upon classical PID techniques and it generates reference forces corresponding to desired lift/pitch/roll/warp motion, whereas the force controller utilizes sliding mode based techniques, and it computes the electronic currents required to track these reference forces.

3.1 AHP description

The quarter–car model of a hydro–pneumatic active suspension is shown in Fig. 2. The cylinder with interior

m_q	Quarter–car weight
C_l	Leaf valve flow conductance
A_z	Cross sectional area of the piston
κ	Adiabatic exponent of the gas
k_v	Valve gain
E	Compression module of oil
V_{z0}	Volume of oil at operating point
p_{sys}, p_{res}	Pressure of system and reservoir
p_z, p_s	Pressure of cylinder and gas spring
q_{sz}	Flow from cylinder into gas spring
q_{zr}	Flow from reservoir into cylinder
w_a	natural frequency of valve
η_a	damping coefficient of valve
d_0, d_1, d_2, d_z	Road, wheel, body and cylinder displacement
I_c	Input current to servo valve

Table 2. Suspension system variables

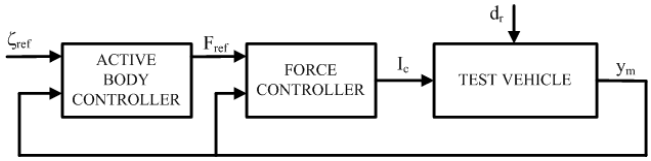

Fig. 3. Vertical controller architecture.

pressure p_z is connected to a gas spring (with pressure p_s) through a laminar resistance with conductance C_l. The oil flow into and out of the cylinder is controlled through a servo valve by applying an electric current I_c. If the control input I_c is positive, then oil is pumped into the cylinder while a negative current results in a flow of oil from cylinder into the reservoir. In [Akar et al., 2007], we have come up with the reduced order model of the AHP system as

$$\begin{aligned}
\ddot{d}_z &= -\frac{a_{21}}{m_q} d_z - \frac{a_{22}+d_v}{m_q}\dot{d}_z - \frac{F_c}{m_q}\mathrm{sign}(\dot{d}_z) + \frac{a_{23}}{m_q} A_z p_z \\
\dot{p}_z &= \frac{E}{V_{z0}} A_z \dot{d}_z - \frac{E}{V_{z0}} C_l (p_z - p_s) + \frac{E}{V_{z0}} q_{zr} \\
\dot{p}_s &= \frac{\kappa C_l}{P_a^{1/\kappa} V_a} p_s^{1+1/\kappa} (p_z - p_s)
\end{aligned} \tag{8}$$

where the oil flow through the servo valve q_{zr} can be accurately modelled by

$$q_{zr} = \begin{cases} k_v \mathrm{sat}(I_c)\sqrt{p_{sys} - p_z} & \text{if } I_c \geq 0, \\ k_v \mathrm{sat}(I_c)\sqrt{p_z - p_{res}} & \text{if } I_c < 0, \end{cases} \tag{9}$$

and p_{sys} is the system pressure that is considerably greater than the cylinder pressure; p_{res} is the reservoir pressure that is close to one bar in normal operating conditions; $\mathrm{sat}(I_c)$ is the saturation function. The parameters of the above model have been determined by validating the experimental data from the test vehicle [Akar et al., 2007].

3.2 Suspension Control Unit

Given the reference signal $\xi_{ref} \in \Re^3$, the task of the vertical dynamics controller is to determine the input currents that are to be applied to the suspension systems so that the desired lift/roll/pitch dynamics are tracked. In order to meet this objective, the controller architecture shown in Fig. 3 is implemented on each tire. The proposed controller loop consists of two sub-controller blocks: The Active Body Controller (ABC) and the Force Controller (FC). For the desired vertical dynamics ξ_{ref} and measurements, the ABC generates a desired force F_{ref} which is then fed into the force controller to determine the input current I_c to be applied to the AHP system.

3.3 Active Body Controller (ABC)

The objective of the active body controller is to generate the *desired* force, $F_{ref} \in \Re^4$, in order to induce some desired displacement on each suspension system. Given the reference signal $\xi_{ref} \in \Re^3$, the task is to design an outer control loop that will track the desired lift/roll/pitch dynamics. Let $e_\xi = \xi_{ref} - \xi$ be the tracking error. The controller is a linear one with the diagonal matrix transfer function

$$C_\xi(s) = \mathrm{diag}\{C_{lift}(s), C_{roll}(s), C_{pitch}(s)\}, \tag{10}$$

where $C_{lift}(s)$, $C_{roll}(s)$, and $C_{pitch}(s)$ are PID type controllers, whose proportionality constants are to be chosen appropriately. The controller output is a 3-dimensional vector, $\mathcal{L}^{-1}(C_\xi(s)E_\xi(s))$, which is then transformed into the references forces

$$\begin{aligned}
F_{ref}(t) = {} & T_R \mathcal{L}^{-1}(C_\xi(s)E_\xi(s)) \\
& -mha_y[\alpha,\, -\alpha,\, 1-\alpha,\, -1+\alpha]^T,
\end{aligned} \tag{11}$$

where T_R is a 4×3 transformation matrix that accounts for the geometry of the actuators on the vehicle; a_y is the measured lateral acceleration at the center of gravity; h is the center of gravity height; and α is a design parameter in the interval $(0, 1)$. The second term

$$-mha_y[\alpha,\, -\alpha,\, 1-\alpha,\, -1+\alpha]^T$$

in (11) is to minimize the effect of the coupling from the lateral dynamics onto the vertical ones, and it is useful to cancel this coupling for faster tracking response. The design parameter α controls the force distribution on the tires ($\alpha = 0.5$ is used in the simulations; this choice corresponds to equal distribution of forces).

Choice of the Controller Parameters The choice of the controller parameters for the ABC relies on the linearized version of the validated model by Akar et al. [2007]. In particular, the plant is given by

$$G(s) = \mathrm{diag}\{G_z(s), G_z(s), G_z(s), G_z(s)\}, \tag{12}$$

where $G_z(s) = \bar{b}/(s^2 + \bar{a}_1 s + \bar{a}_2)$, and the system parameters $\bar{b}$, $\bar{a}_1$, and $\bar{a}_2$ are obtained through experimental data verification. The controller parameters are chosen such that the closed loop transfer function

$$\left(I + G(s)T_R C_\xi(s) T_A^\dagger\right)^{-1} G(s) T_R C_\xi(s), \tag{13}$$

is stable, and the plunger acceleration errors in the human sensitivity range (3-8 Hz) are attenuated. In the implementation of the controller on the test vehicle and also in the nonlinear simulator, several filters have to be used to compensate for noise and measurement offsets.

3.4 Force Controller (FC)

Given a reference force F_{ref} that translates into a reference cylinder pressure $p_{z,ref=F_{ref}/A_z}$, the objective of the force controller is to make the cylinder pressure p_z track the

reference value $p_{z,ref}$. With a slight abuse of notation, in the sequel we will be discussing one dimensional variables corresponding to individual tires. Let

$$e_{p_z} = p_z - p_{z,ref}, \tag{14}$$

$$\sigma = e_{p_z} + \lambda_1 \int_0^t e_{p_z}(\tau) d\tau. \tag{15}$$

First, the desired flow is computed as

$$q^*_{zr} = \frac{V_{z0}}{E} \left(\dot{p}_{z,ref} - \lambda_1 e_{p_z} - \lambda_2 \sigma - M \text{sgn}(\sigma) \right), \tag{16}$$

where λ_1, λ_2 and M are positive controller design parameters. The electronic current to be applied is determined from

$$I^*_c = \begin{cases} \dfrac{q^*_{zr}}{k_v \sqrt{p_{sys} - p_z}} & \text{if } q^*_{zr} \geq 0, \\ \dfrac{q^*_{zr}}{k_v \sqrt{p_z - p_{res}}} & \text{if } q^*_{zr} < 0. \end{cases} \tag{17}$$

It can be shown that the force controller in (17) takes the trajectories to the sliding manifold $\sigma = 0$ in finite time; and both e_{p_z} and $\dot{e}_{p_z}$ converge to zero. Furthermore, error dynamics of the FC is given by

$$\dot{e}_{p_z} + \lambda_1 e_{p_z} = 0. \tag{18}$$

The responsiveness of the FC can be controlled by suitably choosing λ_1.

4. NUMERICAL ANALYSIS

In this section, we investigate the emulation capabilities of the proposed integrated chassis controller via simulations in the advanced car simulator, CASCaDE (Computer Aided Simulation of Car, Driver and Environment) provided by Daimler. CASCaDE is a Fortran-based vehicle simulator that was developed to aid the design of new vehicles [Rau, 2003]. The numerical results to be presented in the sequel is a full 5–body (4 wheels and the body) nonlinear vehicle simulation that also includes the following:

(1) An observer unit for estimation of the side–slip angle
(2) Full sensing and actuation units found on the test vehicle
(3) A cruise controller

Specifically, we consider the emulation of four classes of vehicles: Daimler Smart (compact size vehicle), Commercial van, S–class, and a bus. Due to space limitation, only *bus* emulation results are presented for two types of input: a saturated ramp followed by another ramp in the opposite direction and a sinusoidal input (slalom maneuver). In each case, the peak value of the driver input is such that it induces a lateral acceleration of up to 4 m/s^2 on the test vehicle at a constant speed of 80km/hr. These driver inputs are shown in Fig. 4 in the case of bus emulation.

For the inputs shown in Fig. 4, reference trajectories are generated for the desired side slip angle, yaw rate, and roll angle. The desired values for pitch/warp/lift are set to zero, although for some other automotive applications non–zero values for these variables may also make sense.

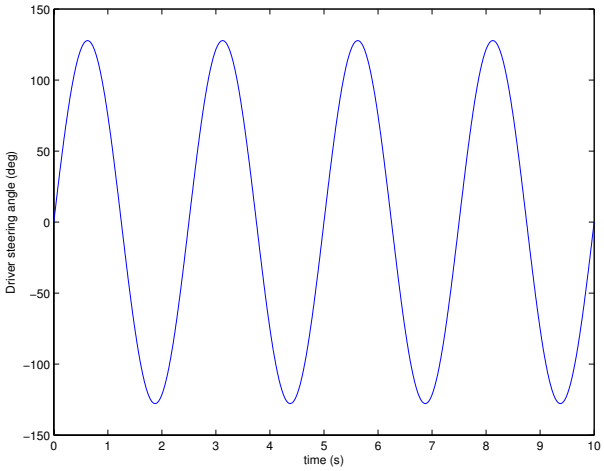

(a)

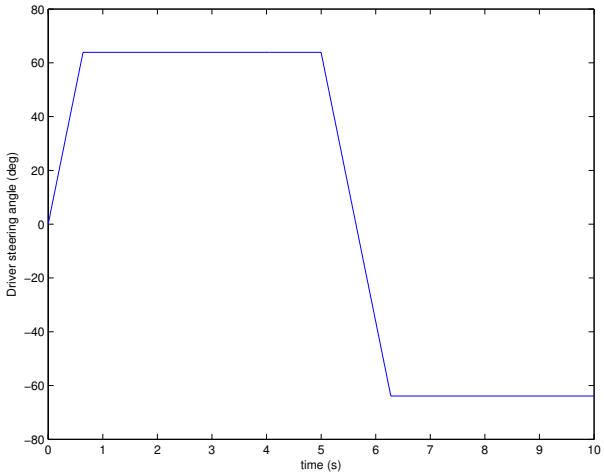

(b)

Fig. 4. Driver inputs used in bus emulation: (a) Slalom maneuver, (b) Double lane change maneuver.

4.1 Slalom Maneuver

The emulation results for the slalom maneuver are summarized in Figs. 5–8. In particular, the lateral dynamics tracking capability and the required steer angles are shown in Figs. 5 and 6, respectively. It is seen that the emulation is quite good despite interaction from vertical dynamics.

Similarly, Figs. 7 and 8 summarize the simulation results for vertical dynamics emulation. As seen in Fig. 7, the roll tracking is pretty good even though such a maneuver creates a lateral acceleration that is at the limit of the linear operation of the vehicle. Furthermore, we note from Fig. 8 that the force tracking is excellent on all suspension systems.

4.2 Double Lane Change Maneuver

The emulation results for the double lane change maneuver (see Fig. 4(b)) are shown in Figs. 9–12. Analogous to the slalom case study, it is seen that both the vertical and lateral dynamics emulation capability seems to be quite amazing.

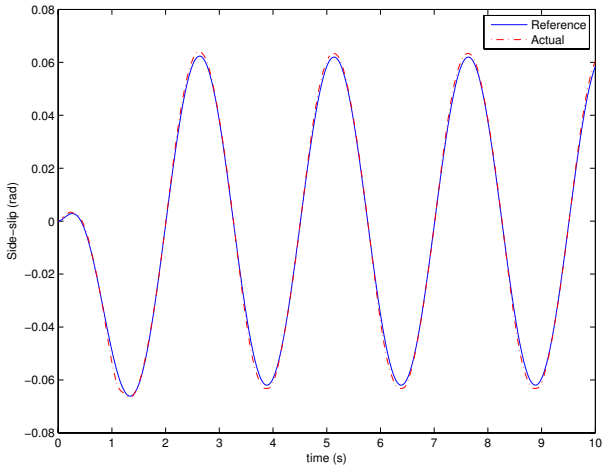

(a)

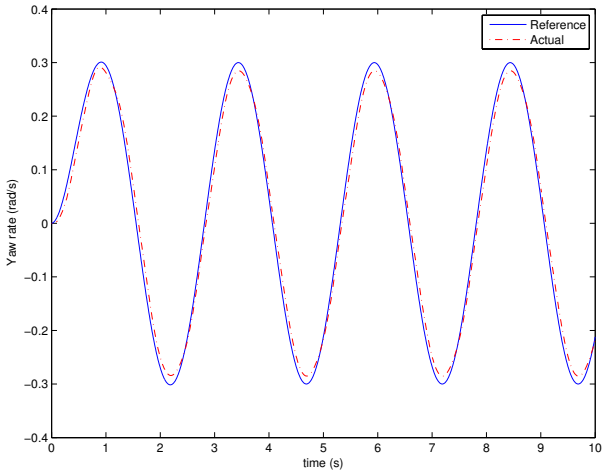

(b)

Fig. 5. Lateral emulation capability for the slalom maneuver: (a) Side–slip angle tracking, (b) Yaw–rate tracking.

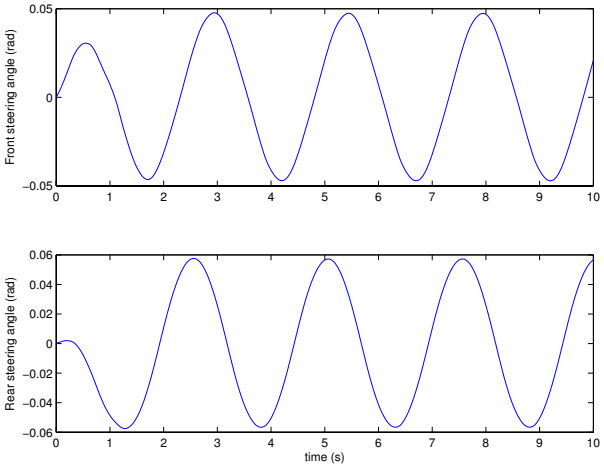

Fig. 6. Required steer angles for the slalom maneuver (bus emulation).

5. CONCLUDING REMARKS

We have presented an integrated chassis controller consisting of 4W–steering and suspension units. Although not all reported here due to space limitation, realistic simulations in CASCaDE demonstrate that the test vehicle can emulate the lateral/vertical dynamics of a broad range of ground vehicles including a van, S–class, and a compact size car. The next step in the evaluation of the proposed controller is to conduct field tests by professional drivers to determine whether, indeed, the feeling of driving another vehicle can be experienced.

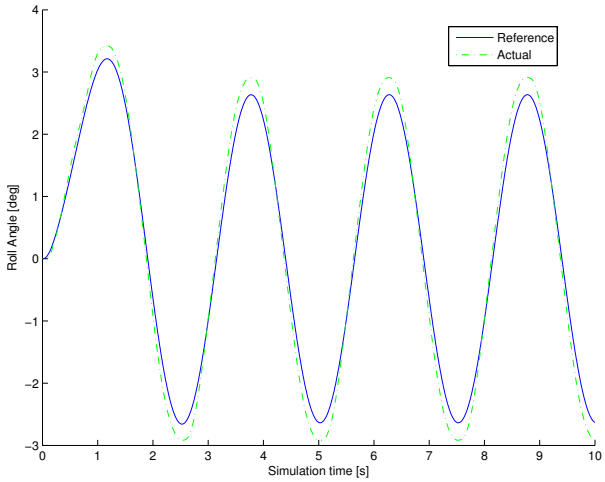

Fig. 7. Roll angle tracking for the slalom maneuver (bus emulation).

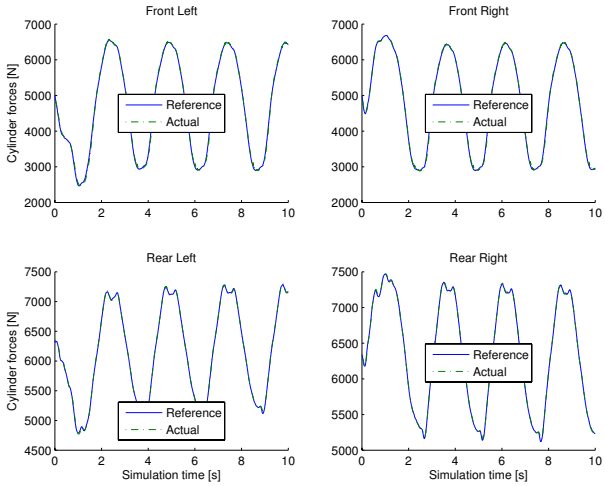

Fig. 8. Force tracking on the suspensions for the slalom maneuver (bus emulation).

REFERENCES

A. Lee. Emulating the lateral dynamics of a range of vehicles using a four-wheel-steering vehicle. SAE Paper No. 950304, *International Congress and Exposition*, Detroit, Michigan, USA, 1995.

Y. Furukawa, N. Yuhara, S. Sano, H. Takeda, and Y. Matsushita. A review of four–wheel steering studies from the viewpoint of vehicle dynamics and control. *Vehicle System Dynamics*, vol. 18, pp. 151–186, 1989.

M. Akar. Yaw rate and sideslip tracking for 4–wheel steering cars using sliding mode control. *Proc. of the IEEE International Conference on Control Applications*, Munich, Germany, October 2006.

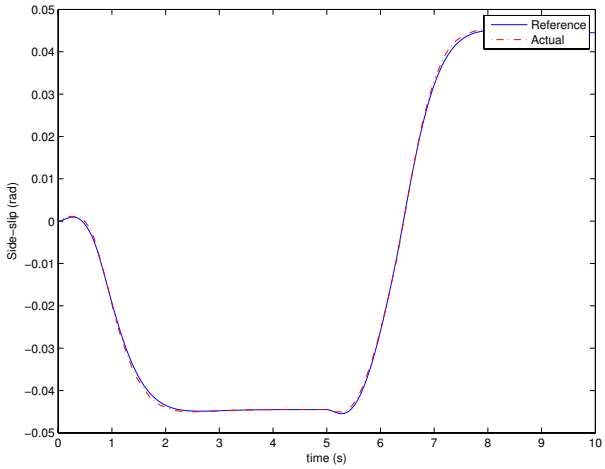

(a)

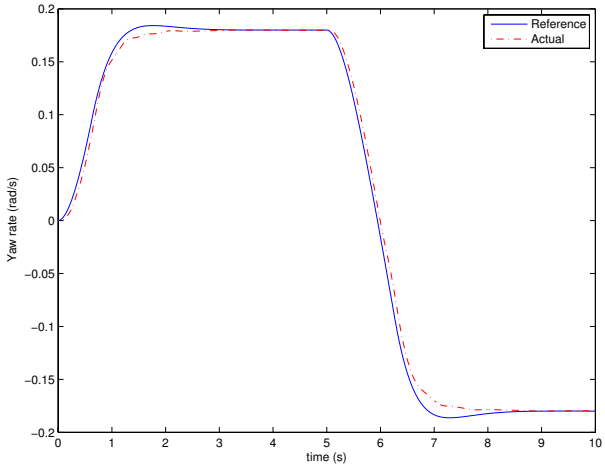

(b)

Fig. 9. Lateral emulation capability for the double-lane change maneuver: (a) Side–slip angle tracking, (b) Yaw–rate tracking.

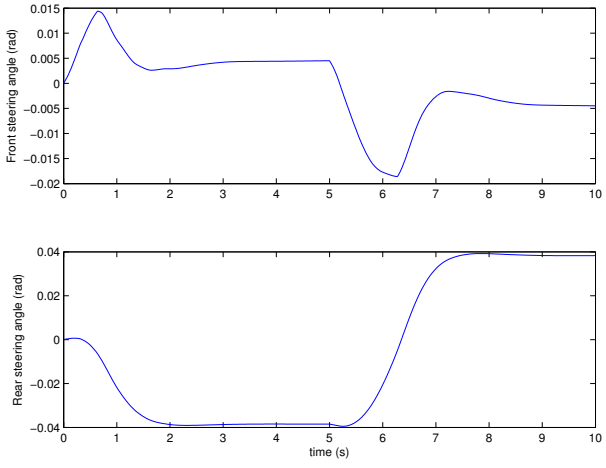

Fig. 10. Required steer angles for the double-lane change maneuver (bus emulation).

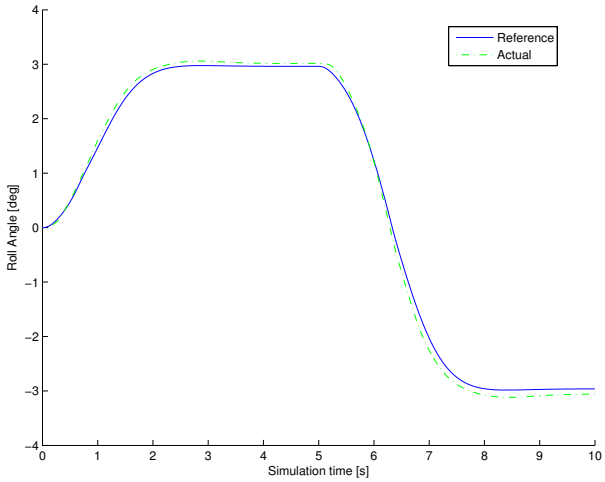

Fig. 11. Roll angle tracking for the double-lane change maneuver (bus emulation).

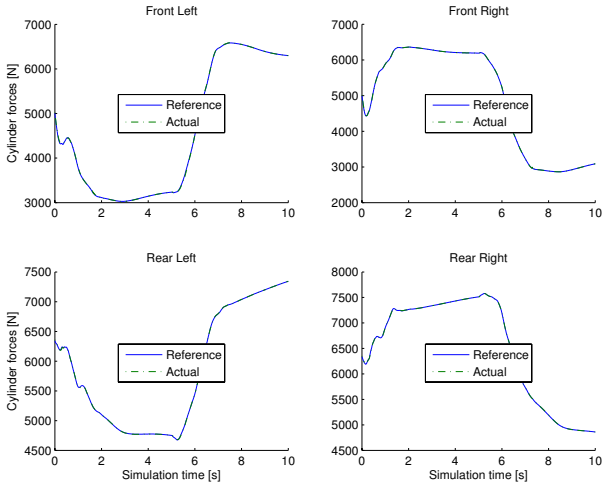

Fig. 12. Force tracking on the suspensions for the double-lane change maneuver (bus emulation).

1990.

E. Duplitzer. *Identifikation und Validierung einers Modells für eing Fahrzeug mit aktivem Fahrwerk*. Studienarbeit, DaimlerBenz, Stuttgart, January 1996.

D. Hrovat. Survey of advanced suspension developments and related optimal control applications. *Automatica*, vol. 33, no. 10, pp. 1781–1817, 1997.

M. Rau. *Modellierung, Simulation and Auslegung eines hydropneumatischen Federbeins mit schnell verstellbarer Dämpfung*. Diplomarbeit, Universität Stuttgart, 2001.

M. C. Smith and F.-C. Wang. Controller parametrization for disturbance response decoupling: Application to vehicle active suspension control. *IEEE Transactions on Control Systems Technology*, vol. 10, no. 3, pp. 393–407, May 2002.

M. Akar, J. C. Kalkkuhl, and A. Suissa. Vertical Dynamics Emulation Using a Vehicle Equipped with Active Suspension. *Proc. of the IEEE Intelligent Vehicles Symposium, Istanbul*, Istanbul, Turkey, June 2007.

J. Rauh. Virtual development of ride and handling characteristics for advanced passenger vehicles. Vehicle System Dynamics, 40(1), pp. 135-155, 2003.

M. Yamashita, K. Fujimoro, C. Uhlik, R. Kawatani and H. Kimura. H_∞ control of an automotive active suspension. *Proceedings of the 29th Conference on Decision and Control*, pp. 2244–2250, Honolulu, Hawaii, December